

# Primordial black hole formation in $k$ -inflation models

Neven Bilić\*

*Division of Theoretical Physics, Rudjer Bošković Institute,  
Zagreb, Croatia*

Dragoljub D. Dimitrijević†, Goran S. Djordjević‡, Milan Milošević§

*Department of Physics, University of Niš, Serbia*

Marko Stojanović¶

*Faculty of Medicine, University of Niš, Serbia*

August 26, 2025

## Abstract

The local primordial density fluctuations caused by quantum vacuum fluctuations during inflation grow into stars and galaxies in the late universe and, if they are large enough, also produce primordial black holes. We study the formation of the primordial black holes in  $k$ -essence inflation models with a potential characterized by an inflection point. The background and perturbation equations are integrated numerically for two specific models. Using the critical collapse and peaks formalism, we calculate the abundance of primordial black holes today.

## 1 Introduction

According to the original idea of Zel'dovich and Novikov [1], highly overdense regions of inhomogeneities in the early universe could gravitationally collapse to form black holes (BHs) [2, 3, 4, 5], the so-called primordial black holes (PBHs) [5, 6]. It has been argued that PBHs may represent a non-negligible component of cold dark matter that provides the seed for the supermassive BHs that populate the universe.

To generate sufficiently large primordial fluctuations during inflation and form superdense regions that can collapse and become PBHs during the radiation-dominated era, the inflationary scalar perturbations need to be amplified by several orders of magnitude on small scales, i.e.,

---

\*bilic@irb.hr

†ddrag@pmf.ni.ac.rs

‡gorandj@junis.ni.ac.rs

§milan.milosevic@pmf.edu.rs

¶marko.stojanovic@pmf.edu.rs

for wavenumbers  $q$  that are large compared with the pivot scale  $q_{\text{CMB}}$  of the cosmic microwave background (CMB). These scales correspond to the late stages of inflation and are well above the values required to be consistent with CMB observations.

An overdense region collapses and forms a PBH when the local value of the density contrast  $\delta = \delta\rho/\rho$  is above the so-called collapse threshold density contrast  $\delta_c$ . With the help of Newton's gravity and Jeans' radius  $R_J \sim c_s/H$ , it was established that PBH forms when the density contrast at the entry of a certain comoving scale  $q$  into the acoustic horizon (i.e., when  $c_s q = aH$ ) exceeds a threshold value  $\delta_c \sim c_s^2$  [7]. Here,  $c_s$  is the speed of sound equal to  $1/\sqrt{3}$  in the case of radiation dominance. The mass of the resulting PBH is approximately equal to the mass within the horizon at the time of formation. Numerical checks for different primordial perturbation profiles show that during radiation dominance, the value for the threshold density contrast  $\delta_c$  is in the range from 0.4 to 2/3 [8, 9, 10].

Depending on the mass, PBHs trigger different observational signals. PBHs lighter than  $\sim 10^{15}$  g are already evaporated today by Hawking radiation and do not exist in today's Universe. Nevertheless, they leave some traces that allow us to investigate how many PBHs might have existed in the early Universe. The abundance of PBHs lighter than  $10^{15}$  g, for example, is constrained by the Big Bang nucleosynthesis since the evaporation of high-energy particles changes the abundance of light elements [11].

PBHs heavier than  $10^{15}$  g have not yet lost their mass significantly by evaporation and remain in the present Universe. They produce various distinct signals at present time, such as

- gravitational lensing,
- dynamical effects on baryonic matter,
- radiation emanating from the accreting matter into PBHs.

The choice of the physical process needed to show the existence of PBHs depends on the BH mass [12, 13, 14, 15, 16, 17]. For instance, gravitational lensing of background stars is the most powerful method to search for sub-solar PBHs. Accretion and dynamical effects on baryonic matter become more important for heavier PBHs.

There are various scenarios for primordial black hole production. We aim to investigate PBH production in the early Universe in two inflation models with noncanonical kinetic terms. The models in which the kinetic term has a noncanonical form are usually referred to as  $k$ -essence [18] or, in the context of inflation,  $k$ -inflation models [19]. In this work, we study two  $k$ -essence models using the Hamiltonian formalism for the background field equations.

First, we investigate a  $k$ -essence model proposed by Papanikolaou, Lymeris, Lola, and Saridakis in Ref. [20]. We will refer to their model as the PLLS model. The PLLS Lagrangian is of the form

$$\mathcal{L} = \left( \frac{g^{\mu\nu}\varphi_{,\mu}\varphi_{,\nu}}{2} \right)^\alpha - U(\varphi), \quad (1)$$

where  $\varphi$  is a scalar field and  $\alpha \geq 0$  is a constant. The same form of  $k$ -essence has recently been studied in the context of the black-bounce solution [21]. The potential  $U$  in Ref. [20] is assumed to be a positive function of  $\varphi$  with a specific inflection point. An inflationary potential with an inflection or near inflection point leads to an ultra slow-roll regime, which in turn leads to a peak in the power spectrum of curvature perturbations on comoving wavenumber scales above the CMB pivot scale  $q_{\text{CMB}}$ . As a result, the enhanced cosmological perturbations could collapse into PBHs [9, 22, 23, 24, 25, 26].

Second, we consider the tachyon inflation model [27, 28, 29, 30, 31, 32, 33, 34, 35, 36, 37, 38, 39, 40]. The first proposals for tachyon inflation models date back to the beginning of this

century, emerging as promising candidates for a natural mechanism to trigger inflation. In our previous works [41, 42, 43, 38, 44], we have studied tachyon inflation in the contexts of the Randall–Sundrum type braneworld cosmology, and have shown that the predicted observational cosmological parameters are in good agreement with Planck data. In this work, we apply the tachyon inflation model to study the formation of PBHs.

The Tachyon model is motivated by low-energy string theory. The existence of tachyons in the perturbative spectrum of string theory shows that the perturbative vacuum is unstable. This instability implies that there exists a true vacuum to which a tachyon field  $\varphi$  tends [45]. The foundations of this process are given by a model of effective field theory [46] with a Lagrangian of the Dirac-Born-Infeld (DBI) form

$$\mathcal{L} = -U(\varphi) \sqrt{1 - g^{\mu\nu} \varphi_{,\mu} \varphi_{,\nu}}. \quad (2)$$

A similar Lagrangian appears in the so-called brane inflation models [47]. In these models, the motion of a D3-brane in a warped throat region of a compact space drives inflation, and the DBI field corresponds to the position of the D3-brane. Here, we assume that the tachyon potential has an inflection point, as in the PLLS case.

To achieve our primary objective, we first calculate the power spectra of the curvature perturbations in the two models mentioned above and demonstrate that the spectra exhibit a substantial enhancement, depending on the input parameters and initial values of the background fields. We calculate the spectra at the acoustic horizon, assuming the Bunch-Davies initial conditions in the deep subhorizon region. Then, using the critical collapse and peaks formalism, we calculate the PBH abundance today that constitutes a fraction of dark matter.

The remainder of the paper is organized as follows. In the next two sections, we investigate the background equations of the PLLS model (Sec. 2) and the Tachyon model (Sec. 3). In Section 4, we study the spectra of curvature perturbations in both models. In Section 5, we present our results on the PBH formation. In the last section, Sec. 6, we summarize our main results and outline conclusions. In Appendix A we outline the procedure for calculating the critical overdensity threshold for collapse.

### Notation

We use the metric signature  $(+, -, -, -)$ . Unless specified otherwise, we use the system of units in which  $c = \hbar = 1$ . For convenience, we introduce a length scale  $\ell$  so that  $\ell \gg 1/M_{\text{Pl}}$ , where  $M_{\text{Pl}} = \sqrt{1/(8\pi G)}$  is the reduced Planck mass. By  $\mathcal{L}$  and  $\mathcal{H}$ , we denote the Lagrangian and Hamiltonian multiplied by  $\ell^4$  so that our  $\mathcal{L}$  and  $\mathcal{H}$  are dimensionless. By  $\varphi$  and  $\phi$ , we denote the scalar fields connected by  $\varphi = \ell^2 \phi$  and have the dimension of length and mass, respectively.

## 2 The PLLS Model

In this section, we briefly recapitulate the model of Ref. [20]. The Lagrangian of this model is a sum of a non-canonical kinetic term and a potential term with inflection,

$$\mathcal{L} = \left( \frac{X}{2} \right)^\alpha - U(\varphi), \quad (3)$$

where we assume that  $X \equiv g^{\mu\nu} \varphi_{,\mu} \varphi_{,\nu}$  is positive. Here,  $\varphi$  is a scalar field of dimension of length, and  $\alpha \geq 1$  is a constant. The physical field  $\phi$ , related to  $\varphi$  via

$$\phi = \varphi / \ell^2, \quad (4)$$

has the usual dimension of mass. The potential with inflection proposed in [20] is given by

$$U = \ell^4 V_0 \left[ \exp \left( -\lambda \frac{|\varphi_0 - \varphi|^n \operatorname{sgn}(\varphi_0 - \varphi)}{\ell^{2n} M_{\text{Pl}}^n} \right) - \exp \left( -\lambda \frac{\varphi_0^n}{\ell^{2n} M_{\text{Pl}}^n} \right) \right]. \quad (5)$$

The quantity  $V_0$  is a constant of the dimension of mass to the 4th power and  $\lambda$  is a positive dimensionless constant. The field shift  $\varphi_0$  corresponds to a shift  $\phi_0$  of the physical field  $\phi$ . This potential has an inflection at  $\varphi = \varphi_0$ .

The background evolution will be studied using the covariant Hamilton formalism. (for details see Ref. [48]). The Hamiltonian corresponding to a  $k$ -essence Lagrangian is obtained by the Legendre transformation

$$\mathcal{H} = 2X\mathcal{L}_X - \mathcal{L}, \quad (6)$$

where the subscript  $X$  denotes a derivative with respect to  $X$ . We find

$$\mathcal{H} = (2\alpha - 1) \left( \frac{X}{2} \right)^\alpha + U(\varphi). \quad (7)$$

As usual, the pressure  $p$  and energy density  $\rho$  are identified with the Lagrangian and the Hamiltonian, respectively. Then, the Hubble expansion rate  $H$  is given by

$$H^2 = \frac{\mathcal{H}}{3\ell^4 M_{\text{Pl}}^2}, \quad (8)$$

and the speed of sound by

$$c_s^2 \equiv \frac{\mathcal{L}_X}{\mathcal{H}_X} = \frac{1}{2\alpha - 1}. \quad (9)$$

Now we introduce the variable  $\eta$  conjugate to  $\sqrt{X}$  as described in [48]

$$\eta = \epsilon \frac{\partial \mathcal{L}}{\partial \sqrt{X}}, \quad (10)$$

where  $\epsilon$  is  $+1$  or  $-1$  according to whether  $\varphi_0$  is positive or negative. In this model, the variable  $X$  can be expressed as an explicit function of  $\eta$ . By making use of (3) and (10) we find

$$\frac{X}{2} = \left( \frac{\eta^2}{2\alpha^2} \right)^{1/(2\alpha-1)}. \quad (11)$$

Then, we obtain the Hamiltonian expressed in terms of  $\varphi$  and  $\eta$  as

$$\mathcal{H} = (2\alpha - 1) \left( \frac{\eta^2}{2\alpha^2} \right)^{\alpha/(2\alpha-1)} + U(\varphi). \quad (12)$$

The first slow roll parameter is given by

$$\varepsilon_1 \equiv -\dot{H}/H^2 = \frac{\mathcal{L} + \mathcal{H}}{2\ell^4 M_{\text{Pl}}^2 H^2} = \frac{3\alpha \left[ \eta^2/(2\alpha^2) \right]^{\alpha/(2\alpha-1)}}{(2\alpha - 1) \left[ \eta^2/(2\alpha^2) \right]^{\alpha/(2\alpha-1)} + U(\varphi)}. \quad (13)$$

The higher order slow roll parameters  $\varepsilon_i$  are defined recursively

$$\varepsilon_{i+1} = \frac{\dot{\varepsilon}_i}{H\varepsilon_i}, \quad i \geq 1. \quad (14)$$

We adopt the convention that inflation ends when either  $\varepsilon_1$  or  $\varepsilon_2$  is close to unity.

The Hamilton equations

$$\dot{\varphi} = \frac{\partial \mathcal{H}}{\partial \eta}, \quad (15)$$

$$\dot{\eta} + 3H\eta = -\frac{\partial \mathcal{H}}{\partial \varphi}. \quad (16)$$

govern the background dynamics. Introducing the e-fold number

$$N = \int dt H, \quad (17)$$

it is convenient to rewrite the Hamilton equations (15) and (16) as differential equations with respect to  $N$ . In this model we find

$$\frac{d\varphi}{dN} = \frac{\eta}{\alpha H} \left( \frac{\eta^2}{2\alpha^2} \right)^{(1-\alpha)/(2\alpha-1)}, \quad (18)$$

$$\frac{d\eta}{dN} = -3\eta - \frac{1}{H} \frac{\partial U}{\partial \varphi}, \quad (19)$$

where

$$H = \frac{1}{\sqrt{3} \ell^2 M_{\text{Pl}}} \left[ (2\alpha - 1) \left( \frac{\eta^2}{2\alpha^2} \right)^{\alpha/(2\alpha-1)} + U(\varphi) \right]^{1/2}. \quad (20)$$

### The Klein-Gordon equation

Instead of the two first-order Hamilton equations, one can use the second-order field equation of motion. This equation can be obtained directly from the Lagrangian or combining Eqs. (18) and (19). Either way one finds<sup>1</sup>

$$\varphi'' + \left( \frac{3}{2\alpha - 1} - \varepsilon_1 \right) \varphi' + \frac{1}{U} \frac{dU}{d\varphi} \frac{3\alpha - (2\alpha - 1)\varepsilon_1}{2\alpha(2\alpha - 1)\varepsilon_1} \varphi'^2 = 0, \quad (21)$$

where

$$\varepsilon_1 = \frac{\alpha}{\ell^2 H^2} \left( \frac{H^2 \varphi'^2}{2} \right)^\alpha, \quad (22)$$

and  $H$  is a solution to

$$\ell^2 H^2 = \frac{1}{\ell^2 M_{\text{Pl}}^2} \left[ (2\alpha - 1) \left( \frac{H^2 \varphi'^2}{2} \right)^\alpha + U(\varphi) \right]. \quad (23)$$

Here and from here on, the prime ' denotes a derivative with respect to  $N$ . The expression (23) is an algebraic equation for the unknown  $H^2$ , so the Klein-Gordon equation (21) involves an implicit function  $H = H(\varphi, \varphi')$ .

---

<sup>1</sup>A comparison with Ref. [20] reveals that the factor  $\alpha(2\alpha - 1)$  in the denominator of the last term on the left-hand side of Eq. (21) is missing in their equation (2.9).

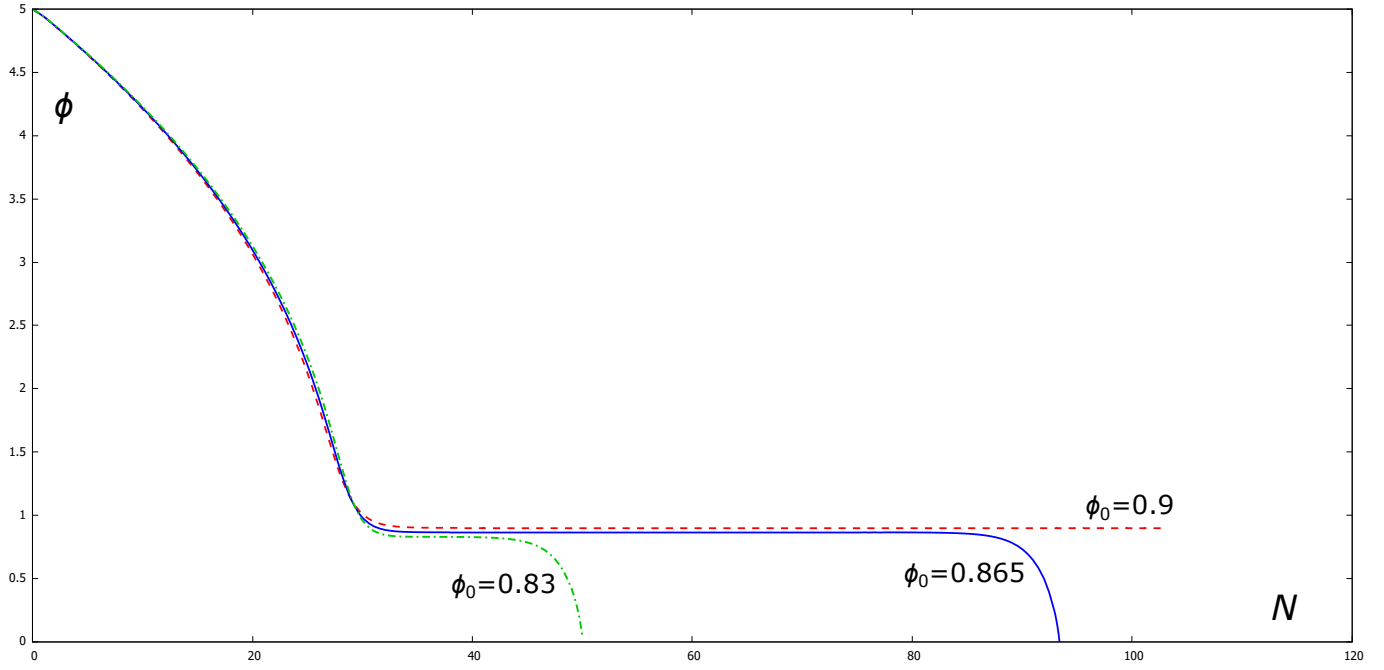


Figure 1: The solution to the Hamilton equations (18) and (19) for the PLLS model. The physical field  $\phi$  in units of  $M_{\text{Pl}}$  is plotted for  $\alpha = 1.5$ , fixed initial  $\phi_{\text{in}} = 5M_{\text{Pl}}$ ,  $\phi'_{\text{in}} = -8 \cdot 10^{-7}M_{\text{Pl}}$  and various  $\phi_0$  in units of  $M_{\text{Pl}}$ . The remaining parameters  $V_0 = 10^{-16}M_{\text{Pl}}^4$  and  $\lambda = 7.54 \cdot 10^{-6}$  are as in Ref [20].

### Input parameters and initial values

The abundance of PBHs depends crucially on the amplitude of the inflationary power spectrum. The initial curvature perturbations will eventually collapse to form BHs if the peak in the amplitude exceeds a certain threshold, which strongly depends on the shape of the curvature spectrum [9]. To achieve a desirable spectrum, it is necessary to tune the input parameters and initial values. However, the tuning of these parameters is not quite arbitrary since the normalization of the curvature spectrum is constrained by its observational value at the pivot CMB scale. As a starting point, we can use the parameterization of Ref. [20] and fix  $\ell = 10^6 M_{\text{Pl}}^{-1}$ ,  $\alpha = 1.5$ ,  $V_0 = 10^{-16}M_{\text{Pl}}^4$ , and  $\lambda = 7.54 \cdot 10^{-6}$  for  $n = 3$ .

Regarding the initial values for  $\varphi$  and  $\eta$ , we first choose  $\phi_{\text{in}}$  and  $\phi'_{\text{in}}$  in units of  $M_{\text{Pl}}$  as in Ref. [20]. Then, the corresponding initial  $\varphi_{\text{in}}$  and  $\varphi'_{\text{in}}$  are obtained using  $\varphi = \ell^2 \phi$ . The corresponding initial  $\eta_{\text{in}}$  is obtained by making use of (18) and numerically solving

$$(\varphi'_{\text{in}})^2 = \frac{6}{M_{\text{Pl}}^2} \frac{x^{2/(2\alpha-1)}}{(2\alpha-1)x^{2\alpha/(2\alpha-1)} + U(\varphi_{\text{in}})} \quad (24)$$

for  $x$ , where

$$x = -\frac{\eta_{\text{in}}}{\sqrt{2\alpha}}. \quad (25)$$

Following Ref. [20], we tune  $\phi_{\text{in}}$  and  $\phi'_{\text{in}}$  to obtain a plateau-like behavior as shown in Fig. 1. These plateau-like solutions are required for a significant PBH production, which we will study in Sec. 5.

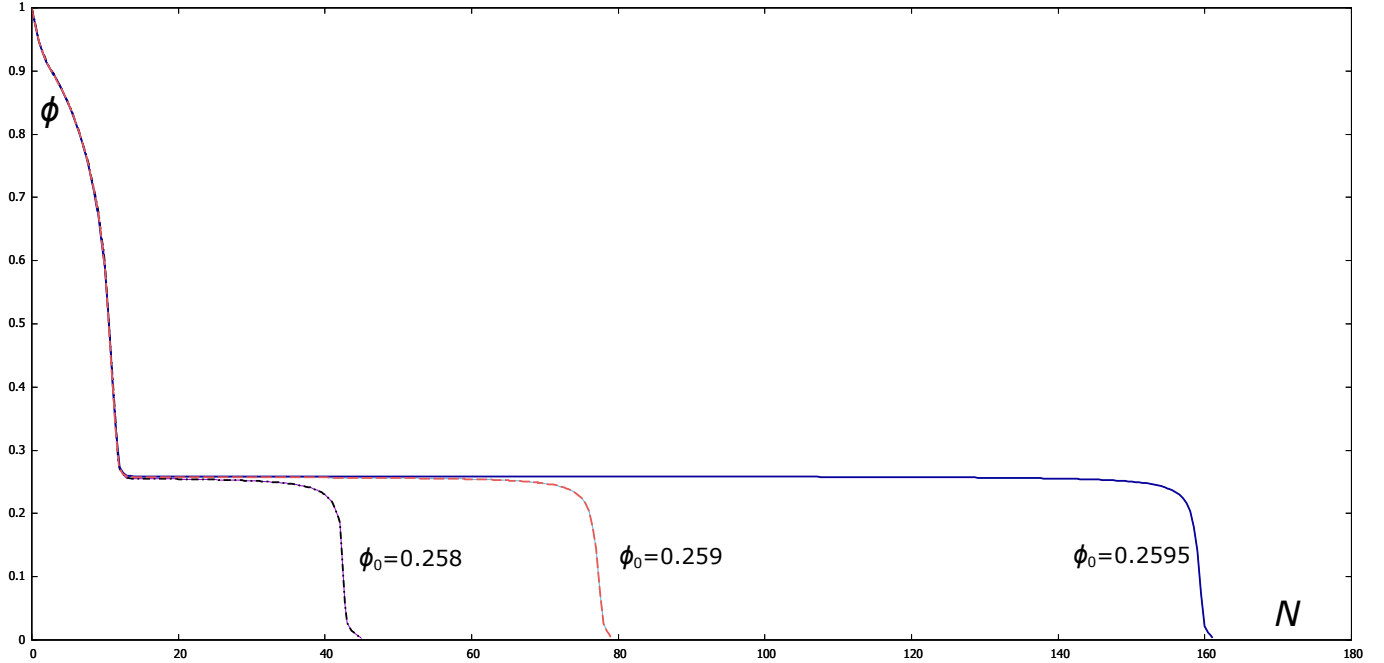


Figure 2: The solution to the Hamilton equations (29) and (30) for the Tachyon model. The physical field  $\phi$  (in units of  $M_{\text{Pl}}$ ) is plotted as a function of  $N$  for  $\phi_{\text{in}} = 1M_{\text{Pl}}$ ,  $\eta_{\text{in}} = -3 \cdot 10^3$ ,  $V_0 = 10^{-16}M_{\text{Pl}}^4$ ,  $\lambda = 7.502 \cdot 10^{-6}$ , and various field shifts  $\phi_0$  in units of  $M_{\text{Pl}}$ , as indicated on the plot.

### 3 The Tachyon model

The Lagrangian in the Tachyon model is given by

$$\mathcal{L} = -U(\varphi)\sqrt{1-X}, \quad (26)$$

where  $U$  is a smooth function of the scalar field  $\varphi$ , and  $X \equiv g^{\mu\nu}\varphi_{,\mu}\varphi_{,\nu} > 0$ . As before, we introduce the conjugate field  $\eta$  related to  $X$  via the definition (10). Using (10) and (26) we obtain  $X$  as a function of the fields  $\varphi$  and  $\eta$

$$X = \frac{\eta^2}{U^2 + \eta^2}. \quad (27)$$

The Hamiltonian can be expressed as a function of either  $X$  or  $\eta^2$ ,

$$\mathcal{H} = \frac{U}{\sqrt{1-X}} = \sqrt{U^2 + \eta^2}. \quad (28)$$

Then, the Hamilton equations (15) and (16), expressed as differential equations with respect to  $N$ , become

$$\frac{d\varphi}{dN} = \frac{\eta}{H\sqrt{U^2 + \eta^2}}, \quad (29)$$

$$\frac{d\eta}{dN} = -3\eta - \frac{U}{H\sqrt{U^2 + \eta^2}} \frac{\partial U}{\partial \varphi}, \quad (30)$$

where the Hubble expansion rate is given by

$$H^2 = \frac{\sqrt{U^2 + \eta^2}}{3\ell^4 M_{\text{Pl}}^2}. \quad (31)$$

The first slow-roll parameter and the speed of sound squared can be expressed as

$$\varepsilon_1 = \frac{3}{2}X = \frac{3}{2} \frac{\eta^2}{U^2 + \eta^2}, \quad (32)$$

$$c_s^2 = 1 - X = \frac{U^2}{U^2 + \eta^2} = 1 - \frac{2}{3}\varepsilon_1. \quad (33)$$

As in the PLLS model, we choose the potential  $U(\varphi)$  defined by (5). The parameters of the potential are  $\ell = 10^6 M_{\text{Pl}}^{-1}$ ,  $n = 3$ , and  $V_0 = 10^{-16} M_{\text{Pl}}^4$  as before. For this model we choose a slightly different  $\lambda = 7.502 \cdot 10^{-6}$ . Regarding the initial values for  $\varphi$  and  $\eta$ , we first choose  $\phi_{\text{in}}$  in units of  $M_{\text{Pl}}$  of the order of those in Ref. [20] with the corresponding  $\varphi_{\text{in}} = \phi_{\text{in}}/\ell^2$ . Then, we tune  $\varphi_{\text{in}}$  and  $\eta_{\text{in}}$  to obtain plateau-like solutions as shown in Fig. 2.

## 4 Curvature perturbations

We start from the 1st-order differential equations of Garriga and Mukhanov [49] expressed in the form [38, 50]

$$a\dot{\xi}_q = z^2 c_s^2 \zeta_q, \quad (34)$$

$$a\dot{\zeta}_q = -z^{-2} q^2 \xi_q, \quad (35)$$

where  $q$  is the comoving wavenumber and  $\zeta_q$  is the Fourier transformed curvature perturbation on uniform-density hyper-surfaces. The quantity  $z^2$  can be expressed in different ways:

$$z^2 = \frac{a^2(p + \rho)}{H^2 c_s^2} = \frac{2M_{\text{Pl}}^2 a^2 \varepsilon_1}{c_s^2} = \frac{a^2 \eta \mathcal{H}_{,\eta}}{\ell^4 H^2 c_s^2} = \frac{a^2 \mathcal{H}_{,\eta}^2}{\ell^4 H^2 \mathcal{H}_{,\eta\eta}}. \quad (36)$$

Here, the subscripts  $\eta$  and  $\eta\eta$  denote respectively the first and second-order partial derivatives with respect to  $\eta$ .

It is convenient to substitute the e-fold number  $N$  for  $t$  using  $dt = dN/H$  and express Eqs. (34)-(35) as differential equations with respect to  $N$ . Then, combining the obtained equations, one can derive the Mukhanov-Sasaki second-order differential equation

$$\frac{d^2 \zeta_q}{dN^2} + \left( 3 + \varepsilon_2 - \varepsilon_1 - 2\frac{c'_s}{c_s} \right) \frac{d\zeta_q}{dN} + \frac{c_s^2 q^2}{a^2 H^2} \zeta_q = 0. \quad (37)$$

Equation (37) is equivalent to the set (34)-(35) with (36). We will integrate Eq. (37) in conjunction with the background Hamilton equations for the two models considered in Secs. 2 and 3.

The perturbations travel at the speed of sound, and their horizon is the acoustic horizon with radius  $c_s/H$ . At the acoustic horizon, the perturbations with the comoving wave number  $q$  satisfy the horizon crossing relation

$$a(N_q)H(N_q) = c_s(N_q)q. \quad (38)$$

In the slow-roll regime, the perturbations are conserved once they cross the horizon from the subhorizon to the superhorizon region. A rough estimate [48] shows that the horizon crossing happens at a relatively large  $q$ -dependent  $N$  of the order  $N_q \sim 7 + \ln q/q_{\text{CMB}}$ , where  $q_{\text{CMB}}$  is the

CMB pivot scale. The curvature perturbations  $\zeta_q$  are approximately constant at large  $N$  once they cross the horizon and enter the superhorizon region where  $a(N)H(N) > c_s(N)q$ ,  $N > N_q$ .

The power spectrum of the curvature perturbations is given by

$$\mathcal{P}_S(q) = \frac{q^3}{2\pi^2} |\zeta_q(N_q)|^2, \quad (39)$$

where  $\zeta_q(N_q)$  is the solution to Eq. (37) taken at the point  $N_q$  which for given  $q$  satisfy (38). The curvature perturbation spectrum needs to satisfy the Harrison-Zeldovich spectrum near  $q = q_{\text{CMB}} = 0.05 \text{ Mpc}^{-1}$

$$\mathcal{P}_S(q) = A_S \left( \frac{q}{q_{\text{CMB}}} \right)^{n_S - 1}, \quad (40)$$

where  $n_S$  is the scalar spectral index and  $A_S = (2.10 \pm 0.03) \times 10^{-9}$ . Since the Mukhanov-Sasaki equation (37) is linear, the requirement

$$\mathcal{P}_S(q_{\text{CMB}}) = \frac{q_{\text{CMB}}^3}{2\pi^2} |\zeta_{q_{\text{CMB}}}(N_{q_{\text{CMB}}})|^2 = A_S \quad (41)$$

can fix the normalization of  $\zeta_q$ .

For convenience, instead of  $\zeta_q$  from now on, we will use the Mukhanov-Sasaki function  $v_q = z\zeta_q$ , where the quantity  $z$  is defined by (36). Then, Eq. (37) may be written as

$$v_q'' + (1 - \varepsilon_1)v_q' + \left[ \frac{c_s^2 q^2}{a^2 H^2} - (2 - \varepsilon_1 + \frac{\varepsilon_2}{2} - \frac{c_s'}{c_s})(1 + \frac{\varepsilon_2}{2} - \frac{c_s'}{c_s}) - \frac{\varepsilon_2 \varepsilon_3}{2} + (\frac{c_s'}{c_s})' \right] v_q = 0. \quad (42)$$

Note that in the PLLS model  $c_s'$  vanishes whereas in the Tachyon model, we have

$$\frac{c_s'}{c_s} = -\frac{\varepsilon_1 \varepsilon_2}{3 - 2\varepsilon_1}, \quad (43)$$

$$(\frac{c_s'}{c_s})' = -\frac{(\varepsilon_1 \varepsilon_2^2 + \varepsilon_1 \varepsilon_2 \varepsilon_3)(3 - 2\varepsilon_1) + 2\varepsilon_1^2 \varepsilon_2^2}{(3 - 2\varepsilon_1)^2}. \quad (44)$$

To solve Eq. (42), we need to choose the initial point  $N_{\text{in},q}$  for each wavenumber  $q$ . The appropriate  $q$ -dependent initial point must be in the deep subhorizon region where  $a_{\text{in}}H_{\text{in}} \ll c_s q$ . More precisely, for each wave number  $q$  that satisfies the horizon crossing relation  $a(N_q)H(N_q) = c_s(N_q)q$ , we start at a  $q$ -dependent  $N_{\text{in},q} < N_q$  such that

$$a(N_{\text{in},q})H(N_{\text{in},q}) = \beta c_s(N_{\text{in},q})q, \quad (45)$$

where  $\beta$  is a small parameter, e.g.,  $\beta = 0.01$  as proposed in Ref. [51]. Owing to the  $N$ -translation invariance of the background equations, we could choose an arbitrary origin of inflation  $N_0$  as an initial point related to a wavenumber  $q_0 < q_{\text{CMB}}$ . In other words, we set

$$a_0 H_0 = \beta c_{s0} q_0 = \epsilon c_{s0} q_{\text{CMB}}, \quad (46)$$

where  $a_0 = a(N_0)$ ,  $H_0 = H(N_0)$ ,  $c_{s0} = c_s(N_0)$ , and the small parameter  $\epsilon$  satisfies  $\epsilon < \beta$ , e.g.,  $\epsilon = 0.001$ . Then, using  $a = a_0 e^{N - N_0}$  together with (46), we can write the first term in the square brackets in Eq. (42) as

$$\frac{c_s^2 q^2}{a^2 H^2} = \frac{e^{2N_0 - 2N}}{\epsilon^2} \frac{c_s^2}{c_{s0}^2} \frac{H_0^2}{H^2} \frac{q^2}{q_{\text{CMB}}^2}. \quad (47)$$

For more details on the choice of the initial point, see Ref. [48].

To find the spectrum at the horizon crossing, equation (42) should be integrated for a fixed  $q$  up to the e-fold number  $N_q$ , which satisfies the horizon-crossing equation (38). Fixing the beginning of inflation at  $N_0 = 0$  and combining Eqs. (38) and (46) we obtain

$$e^{N_q} = \frac{1}{\epsilon} \frac{q}{q_{\text{CMB}}} \frac{H_0}{H(N_q)} \frac{c_s(N_q)}{c_{s0}}, \quad (48)$$

which, given  $q$ , may be regarded as an algebraic equation for  $N_q$ . The explicit functional dependence  $H(N_q)$  and  $c_s(N_q)$  in (48) is obtained by integrating the background Hamilton equations in parallel with (42). Then, the spectrum  $\mathcal{P}_S(q)$  can be plotted using the solutions  $\zeta_q(N_q)$  at the point  $N_q$  that satisfies (48) for each  $q$ .

## Initial conditions

To determine the proper initial conditions in the deep subhorizon region, we adopt the standard Bunch-Davies vacuum solution [52]

$$v_q(\tau) = \frac{e^{-ic_s q \tau}}{\sqrt{2c_s q}}, \quad (49)$$

where the conformal time  $\tau = \int dt/a$  in the slow-roll regime satisfies

$$\tau = -\frac{1 + \varepsilon_1}{aH} + \mathcal{O}(\varepsilon_1^2), \quad (50)$$

with  $-qc_s\tau \gg 1$  in the deep subhorizon region. Hence, the initial values of  $v_q$  and  $v'_q$  at  $N_{\text{in},q}$  are determined by (49) up to an arbitrary phase. The simplest choice is

$$v_{q\text{in}} \equiv v_q(N_{\text{in},q}) = \frac{1}{\sqrt{2c_s q}}, \quad (51)$$

$$v'_{q\text{in}} \equiv v'_q(N_{\text{in},q}) = -i \frac{c_s q}{a(N_{\text{in},q}) H(N_{\text{in},q}) \sqrt{2c_s q}}. \quad (52)$$

Then, using (45), we have

$$v'_{q\text{in}} = -i \frac{1}{\beta \sqrt{2c_s q}}, \quad (53)$$

where  $\beta$  is a small constant discussed above, e.g.,  $\beta = 0.01$ . It is understood that the function  $c_s$  in Eqs. (51)-(53) is taken at  $N = N_{\text{in},q}$ .

## 4.1 Redefinition of the input parameters and fields

In our calculations, we assume certain values of the parameters and initial values of the fields. Besides, a solution to Eq. (42) involves the Bunch-Davies initial conditions (51) and (52). These initial conditions determine the normalization of  $\zeta_q(N)$  which in turn fixes the normalization of  $\mathcal{P}_S$ . Hence, there is *a priori* no guarantee that the obtained spectrum will satisfy the condition (41). Instead, the obtained spectrum  $\mathcal{P}_S$  will satisfy

$$\mathcal{P}_S(q_{\text{CMB}}) = \frac{A_s}{c_0}, \quad (54)$$

Table 1: Input parameters and fields

PLLS model, $\alpha = 1.5$		Tachyon model	
original	redefined	original	redefined
$U$	$c_0^{-1}U$	$U$	$c_0^{-1}U$
$\lambda$	$c_0^{(1-\alpha)/(2\alpha)}\lambda$	$\lambda$	$c_0^{-1/2}\lambda$
$\varphi$	$c_0^{(\alpha-1)/(2\alpha)}\varphi$	$\varphi$	$c_0^{1/2}\varphi$
$\eta$	$c_0^{(1-2\alpha)/(2\alpha)}\eta$	$\eta$	$c_0^{-1}\eta$

where  $c_0$  is a constant, generally  $c_0 \neq 1$ . Thus, we have a conflict between the imposed Bunch-Davies vacuum and the normalization of the spectrum to the observed value at the CMB pivot scale.

To rectify this conflict, we need to properly redefine the input parameters and initial values. Using an arbitrary constant  $c_0$ , one may easily show [48] that the Hamilton equations and the corresponding solutions are invariant under the simultaneous rescaling of the parameters and initial values as shown in Table 1. In both models, the Hubble rate scales according to  $H \rightarrow c_0^{-1/2}H$  and the rescaled Hamilton equations retain their original form with no dependence on  $c_0$ .

We will use this scaling property of our  $k$ -essence models to eliminate the constant  $c_0$  in Eq. (54) by redefining the input parameters. To begin, we multiply the right-hand side of (39) by  $c_0$  and write the power spectrum  $\mathcal{P}_S$  as

$$\mathcal{P}_S = c_0 \frac{q^3}{2\pi^2} |\zeta_q(N_q)|^2 = \frac{c_0 H^2}{4\pi^2 \varepsilon_1 M_{\text{Pl}}^2} q |v_q|^2, \quad (55)$$

where we have used Eqs. (36) and (38). Now we absorb  $c_0$  in  $H^2$  and rescale the Hubble rate as  $H \rightarrow c_0^{-1/2}H$ . This rescaling does not affect Eq. (42) and its solution  $v_q$ . Thus, we obtain a properly normalized spectrum without the  $c_0$  factor. However, a rescaling of  $H$  implies a redefinition of the model input parameters and initial values of the background fields. Using the rescaling defined in Table 1 we infer a redefinition of the parameters.

In this way, if we repeat the calculations using the redefined input parameters listed in Table 1 for both models, we will obtain the power spectra that agree with the observed value at the CMB pivot scale.

## 4.2 Approximate spectrum

In the slow-roll regime, the curvature spectrum can be approximated by (see, e.g., Ref. [50])

$$\mathcal{P}_S(q) \simeq \frac{1}{8\pi^2 c_s \varepsilon_1} \frac{H^2}{M_{\text{Pl}}^2}, \quad (56)$$

where for each  $q$ , the quantities  $H$ ,  $c_s$ , and  $\varepsilon_1$  take on their horizon crossing values at the corresponding  $N_q$ . The approximate spectrum obtained in this way will not in general have the correct observed value at the pivot scale  $q_{\text{CMB}}$ . To satisfy the proper normalization of  $\mathcal{P}_S(q)$  at  $q = q_{\text{CMB}}$ , we can introduce a constant factor  $\bar{c}_0$ . To wit, we define

$$\mathcal{P}_S(q) \simeq \frac{\bar{c}_0}{8\pi^2 c_s \varepsilon_1} \frac{H^2}{M_{\text{Pl}}^2} \quad (57)$$

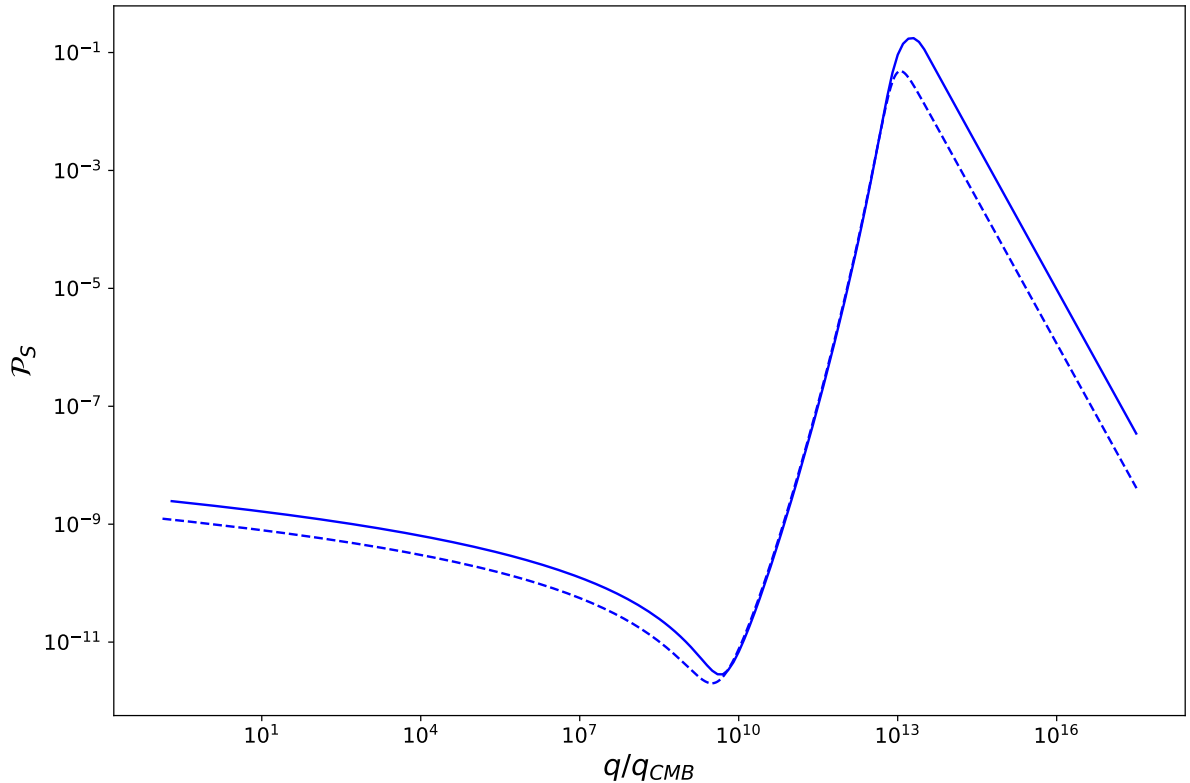


Figure 3: The curvature power spectrum obtained by numerically solving Eq. (42) (full line) and the spectrum approximated by Eq. (57) (dashed line) for the PLLS inflation model with  $n = 3$ ,  $\phi_0 = 0.8354M_{\text{Pl}}$ , and  $\alpha = 1.5$ . The values of  $V_0$  and  $\lambda$  are as in Fig. 1. The initial values are  $\phi_{\text{in}} = 5.20473M_{\text{Pl}}$ ,  $\eta_{\text{in}} = -2.81744 \cdot 10^{-7}$ . The initial perturbation  $v_{q\text{in}}$  is determined by the Bunch-Davies vacuum and  $\mathcal{P}_S(q_{\text{CMB}})$  as discussed in the text.

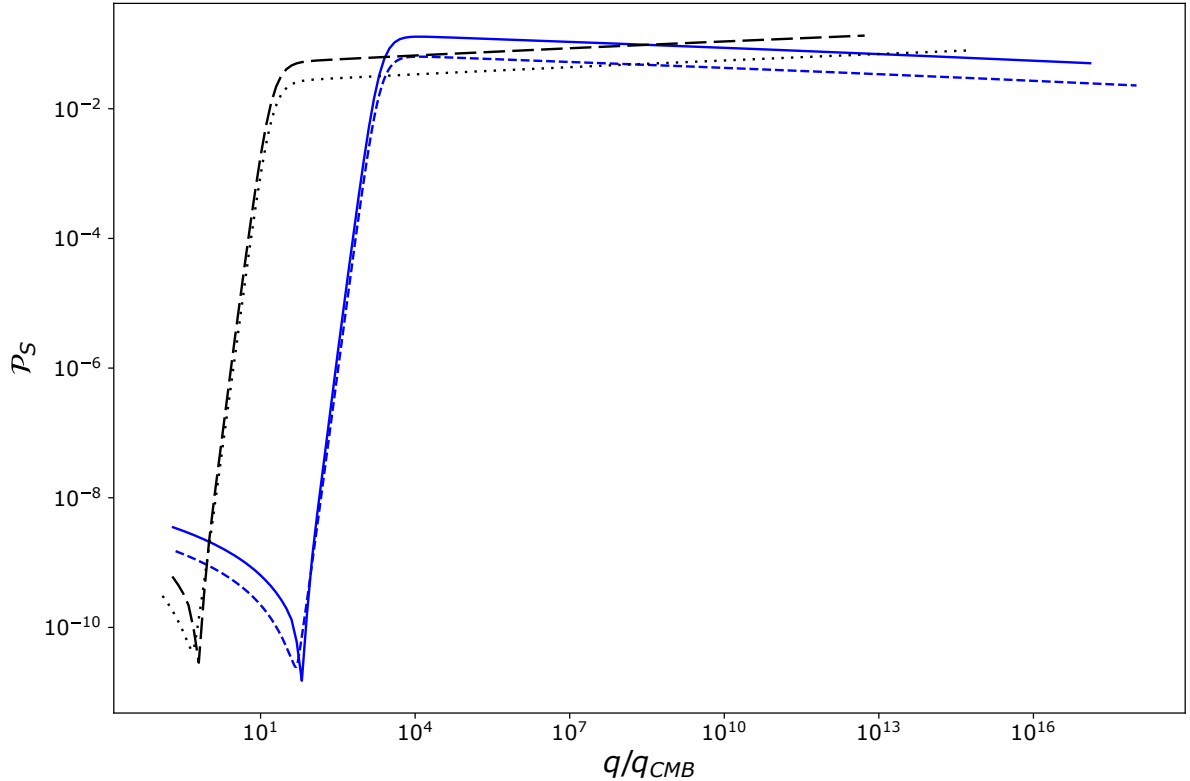


Figure 4: The curvature power spectrum obtained by numerically solving equation (42) (full blue and long-dashed black lines) combined with the spectrum approximated by Eq. (57) (short dashed blue and dotted black lines) for the Tachyon model inflation with the potential  $U$  as in the PLLS model. The parameters and initial values of the corresponding background solutions are  $\phi_0 = 0.2595 M_{\text{Pl}}$ ,  $V_0 = 10^{-16} M_{\text{Pl}}^4$ ,  $\lambda = 7.502 \cdot 10^{-6}$ ,  $\phi_{\text{in}} = 1.1 M_{\text{Pl}}$ , and  $\eta_{\text{in}} = -5.3 \cdot 10^4$  (full and short-dashed lines), and  $\phi_0 = 0.259831 M_{\text{Pl}}$ ,  $V_0 = 10^{-16} M_{\text{Pl}}^4$ ,  $\lambda = 7.600 \cdot 10^{-6}$ ,  $\phi_{\text{in}} = 1.052 M_{\text{Pl}}$  and  $\eta_{\text{in}} = -5.3625 \cdot 10^4$  (long-dashed and dotted lines).

and fix  $\bar{c}_0$  so that  $\mathcal{P}_S(q_{\text{CMB}})$  has the correct observed value at the pivot scale. However, a choice  $\bar{c}_0 \neq 1$  is not compatible with the assumed Bunch-Davies asymptotic behavior. As before, this problem is resolved by absorbing  $\bar{c}_0$  in  $H^2$  and redefining the physical parameters as shown in Table 1.

**Nota Bene:** The constants  $c_0$  and  $\bar{c}_0$  need not be necessarily equal. However, to compare the exact and approximate spectra, we must stick to the same parameterization of the model in both exact and approximate calculations. In this case, we will replace  $\bar{c}_0$  in (57) by  $c_0$  so that the redefinition of parameters and initial values will be the same. Obviously, in this case, the approximate spectrum will fail to reproduce the correct observed value at  $q = q_{\text{CMB}}$ .

We plot the calculated spectrum for the PLLS model in Fig. 3. In Fig. 4, we plot the spectra calculated for the Tachyon model for two sets of parameters. The approximation (56) correctly reproduces the shape of the spectrum but underestimates the peak by a factor of the order of 10 and violates the normalization condition (41) (see the note after Eq. (57)).

## 5 PBH formation

In the radiation-dominated epoch, PBHs could form by small-scale cosmological perturbations with sufficiently large overdensities collapsing after re-entering the cosmological horizon. Assuming spherical symmetry, such regions can be described by the following approximate form of the metric at superhorizon scales [8]

$$ds^2 = dt^2 - a(t)^2 e^{2\zeta(r)} (dr^2 + r^2 d\Omega^2). \quad (58)$$

The quantity  $\zeta(r)$  is spherically symmetric comoving curvature perturbation conserved on superhorizon scales [53]. The corresponding density contrast is given by [9]

$$\delta_r = -\frac{8}{9} \frac{1}{a^2 H^2} e^{-5\zeta(r)/2} \nabla^2 e^{\zeta(r)/2} \simeq -\frac{4}{9} \frac{1}{a^2 H^2} \nabla^2 \zeta(r), \quad (59)$$

or in the momentum space

$$\delta_q \simeq \frac{4}{9} \frac{q^2}{a^2 H^2} \zeta_q. \quad (60)$$

The power spectrum of the density contrast is then

$$P_\delta \equiv \frac{q^3}{2\pi^2} |\delta_q|^2 = \frac{q^3}{2\pi^2} \left(\frac{4}{9}\right)^2 \frac{q^4}{a^4 H^4} |\zeta_q|^2 = \left(\frac{4}{9}\right)^2 \frac{q^4}{a^4 H^4} \mathcal{P}_S. \quad (61)$$

We also define the smoothed variance of the density contrast over the smoothing scale  $R = 1/(aH)$

$$\sigma(R)^2 = \int_0^\infty \frac{dq}{q} W(q, R)^2 P_\delta = \left(\frac{4}{9}\right)^2 \int_0^\infty \frac{dq}{q} (Rq)^4 W(q, R)^2 \mathcal{P}_S \quad (62)$$

and the first moment of the smoothed power spectrum

$$\mu(R)^2 = \int_0^\infty \frac{dq}{q} (Rq)^2 W(q, R)^2 P_\delta = \left(\frac{4}{9}\right)^2 \int_0^\infty \frac{dq}{q} (Rq)^6 W(q, R)^2 \mathcal{P}_S, \quad (63)$$

where  $W$  is a smoothing window function

$$W(q, R) = e^{-q^2 R^2/2}. \quad (64)$$

## Toy model

For an illustration, it is useful to consider a flat power spectrum parameterized as

$$\mathcal{P}_S \simeq \mathcal{P}_0 \Theta(q - q_{\min}) \Theta(q_{\max} - q). \quad (65)$$

This power spectrum, which was studied previously in the literature as a toy model (see, e.g., [54]), can serve as a rough approximation to the Tachyon model power spectrum of Fig. 4 with  $\mathcal{P}_0 \simeq 0.1 - 0.2$ ,  $q_{\min} = 10^4 q_{\text{CMB}}$ , and  $q_{\max} = 10^{16} q_{\text{CMB}}$ .

Using this in (62) and (63) we obtain

$$\sigma^2 = \frac{1}{2} \left( \frac{4}{9} \right)^2 \mathcal{P}_0 \left[ (1 + q_{\min}^2 R^2) e^{-q_{\min}^2 R^2} - (1 + q_{\max}^2 R^2) e^{-q_{\max}^2 R^2} \right], \quad (66)$$

$$\mu^2 = \frac{1}{2} \left( \frac{4}{9} \right)^2 \mathcal{P}_0 \left[ (2 + 2q_{\min}^2 R^2 + q_{\min}^4 R^4) e^{-q_{\min}^2 R^2} - (2 + 2q_{\max}^2 R^2 + q_{\max}^4 R^4) e^{-q_{\max}^2 R^2} \right]. \quad (67)$$

The functions  $\sigma(R)$  and  $\mu(R)$  have a top-hat shape with plateau heights  $\sigma_{\max} \simeq (4/9)\sqrt{\mathcal{P}_0/2}$  and  $\mu_{\max} \simeq (4/9)\sqrt{\mathcal{P}_0}$ . For  $R$  satisfying  $1/q_{\max} \ll R \ll 1/q_{\min}$  we have

$$\sigma = \frac{4}{9} \sqrt{\frac{\mathcal{P}_0}{2}} (1 + q_{\min}^2 R^2 + \mathcal{O}(q_{\min}^4 R^4)), \quad (68)$$

and hence, the maximal value of sigma is

$$\sigma_{\max} \simeq \frac{4}{9} \sqrt{\frac{\mathcal{P}_0}{2}}. \quad (69)$$

In this range of  $R$ , we also have

$$\frac{\mu}{\sigma} \simeq \sqrt{2} + \mathcal{O}(q_{\min}^4 R^4). \quad (70)$$

## Functional dependence $R(M)$

Through (62), the variance  $\sigma$  is a function of the comoving horizon radius at the PBH formation time  $R = (a_f H_f)^{-1} = 1/q_f$ , where the subscript f refers to the PBH formation time. Since the PBH mass  $M$  at the formation time is of the order of the cosmological horizon mass, i.e.,

$$M \simeq M_{H_f} = \frac{4\pi}{3} H_f^{-3} \rho_f = \frac{4\pi M_{\text{Pl}}^2}{H_f}, \quad (71)$$

we can relate  $R$  to  $M$ . From now on, we identify  $M \equiv M_{H_f}$ .

As a first step, we derive the PBH mass  $M$  as a function of the comoving wave number  $q_f$  at the PBH formation time. Combining the entropy conservation  $S = C_1 g_* T^3 a^3 = \text{const}$  with radiation energy density  $\rho_{\text{rad}} = C_2 g_* T^4$ , we find

$$\frac{\rho_{\text{rad},f}}{\rho_{\text{rad},0}} = \left( \frac{g_{*,0}}{g_{*,f}} \right)^{1/3} \left( \frac{a_0}{a_f} \right)^4, \quad (72)$$

where the quantity  $g_*$  is the time-dependent number of effective massless degrees of freedom. Then, from the first Friedmann equation it follows that the Hubble rate  $H_f$  at the formation time is related to the Hubble rate  $H_0$  at present as

$$H_f = H_0 \Omega_{\text{rad},0}^{1/2} (a_0/a_f)^2 (g_{*,0}/g_{*,f})^{1/6}, \quad (73)$$

where  $\Omega_{\text{rad},0} = \rho_{\text{rad},0}/\rho_{\text{crit}}$ , with  $\rho_{\text{crit}} = 3M_{\text{Pl}}^2 H_0^2$ . Combining this with the horizon-crossing relations  $q_f = a_f H_f$  and  $q_0 = a_0 H_0$ , we find

$$\frac{a_f}{a_0} = \Omega_{\text{rad},0}^{1/2} \left( \frac{g_{*,0}}{g_{*,f}} \right)^{1/6} \frac{q_0}{q_f}. \quad (74)$$

Next, substituting  $H_f$  from (73) and  $a_f$  from (74) in  $M = 4\pi M_{\text{Pl}}^2/H_f$ , we find

$$M = \frac{4\pi M_{\text{Pl}}^2}{H_0} \Omega_{\text{rad},0}^{1/2} \left( \frac{g_{*,0}}{g_{*,f}} \right)^{1/6} \left( \frac{q_0}{q_f} \right)^2 = 1.90 \cdot 10^{15} \left( \frac{q_{\text{CMB}}}{q_f} \right)^2 M_{\odot}. \quad (75)$$

For the numerical estimate in (75), we have used  $M_{\text{Pl}} = 2.17645/\sqrt{8\pi} \times 10^{-8}$  kg,  $\Omega_{\text{rad},0} = 10^{-5}$ , the Hubble radius today  $1/H_0 = 1.2 \cdot 10^{26}$  m,  $g_{*,f} = 106.75$ ,  $g_{*,0} = 3.36$  (see, e.g., Kolb and Turner [55]), and the solar mass  $M_{\odot} = 2 \cdot 10^{30}$  kg.

Finally, using (75) with  $a_0 = 1$  we find

$$R \equiv \frac{1}{q_f} = \frac{M^{1/2}}{(4\pi H_0)^{1/2} M_{\text{Pl}}} \left( \frac{g_{*,f}}{g_{*,0}} \right)^{1/12} \Omega_{\text{rad},0}^{-1/4}. \quad (76)$$

It is convenient to express  $R$  as a function of  $M/M_{\odot}$ ,

$$R = 1.4163 \cdot 10^{16} \left( \frac{M}{M_{\odot}} \right)^{1/2} \text{ m} = 4.590 \cdot 10^{-7} \left( \frac{M}{M_{\odot}} \right)^{1/2} \text{ Mpc}. \quad (77)$$

## Estimate of the mass range

Suppose the spectrum is significant between  $q_{\min}$  and  $q_{\max}$  as in the toy model (65). Inspired by the Tachyon model inflation spectrum depicted in Fig. 4 we use  $q_{\min} = 10^4 q_{\text{CMB}}$ ,  $q_{\max} = 10^{16} q_{\text{CMB}}$ . Then, the BH production will be suppressed for  $R > R_{\max} = 1/q_{\min}$  and  $R < R_{\min} = 1/q_{\max}$ . The masses corresponding to  $R_{\min}$  and  $R_{\max}$  are

$$M_{\min} = \left( \frac{R_{\min}}{4.59 \cdot 10^{-7}} \right)^2 \simeq 1.91 \cdot 10^{-17} M_{\odot}, \quad (78)$$

$$M_{\max} = \left( \frac{R_{\max}}{4.59 \cdot 10^{-7}} \right)^2 \simeq 1.91 \cdot 10^7 M_{\odot}. \quad (79)$$

Then, according to (66), the function  $\sigma(M)$  will have an approximate top hat profile with  $M$  ranging from  $M_{\min}$  to  $M_{\max}$  and the top value  $\sigma_{\max}$  defined by (69).

## 5.1 PBH mass fraction

The density of PBHs of mass  $M$  at the formation time is a fraction  $\beta(M)$  of the total background density  $\rho_{\text{rad},f}$ ,

$$\rho_{\text{PBH},f} = \beta(M) \rho_{\text{rad},f}. \quad (80)$$

We now describe two ways of calculating  $\beta(M)$  that appear in the literature: The Press-Schechter and the Critical collapse and peaks (CCP) formalism, and compare the two approaches using the toy-model spectrum.

## Press-Schechter formalism

In the Press-Schechter formalism of gravitational collapse, the mass fraction of PBHs of mass  $M$  is given by the probability that the overdensity  $\delta$  is above a certain threshold value  $\delta_c$  for collapse. Assuming  $\delta$  is a Gaussian random variable with mass (or scale) dependent variance, the mass fraction  $\beta(M)$  at the time of formation is then given by [56, 57, 58]

$$\beta(M) = \frac{1}{2} \operatorname{erfc} \left( \frac{\delta_c}{\sqrt{2}\sigma} \right) \equiv \frac{1}{\sqrt{2\pi}\sigma} \int_{\delta_c}^{\infty} d\delta \exp \left( -\frac{\delta^2}{2\sigma^2} \right). \quad (81)$$

This function can be approximately expressed in terms of elementary functions by [59]

$$\beta(M) \simeq \frac{\exp(-\delta_c^2/(2\sigma^2))}{\sqrt{\pi\delta_c}/(\sqrt{2}\sigma) + \sqrt{\pi\delta_c^2/(2\sigma^2) + 4}}. \quad (82)$$

## Critical collapse and peaks (CCP) formalism

Given linear density contrast  $\delta$ , the PBH mass can be well approximated by the scaling law for critical collapse [60, 61]

$$M_{\text{PBH}}(\delta) = KM(\delta_m(\delta) - \delta_c)^\gamma, \quad (83)$$

where  $\delta_m$  is the smoothed density contrast,  $M \equiv M_{H_f}$  is the mass within the cosmological horizon at the PBH formation time  $t_f$  in radiation era, and  $\gamma \simeq 0.36$  is the critical exponent at  $t_f$  [62]. The parameter  $K \simeq 4$  depends on the specific profile of the collapsing overdensity. The smoothed density contrast  $\delta_m$  may be expressed in terms of  $\delta$  as [61]

$$\delta_m = \delta - \frac{3}{8}\delta^2. \quad (84)$$

Then, the PBH mass fraction is [61]

$$\beta(M) = \int_{\delta_-}^{4/3} d\delta \frac{M_{\text{PBH}}(\delta)}{M} N(\delta), \quad (85)$$

where

$$N(\delta) = \frac{1}{4\pi^2} \left( \frac{\mu\delta}{\sigma^2} \right)^3 \exp \left( -\frac{\delta^2}{2\sigma^2} \right) \quad (86)$$

and the lower integral bound

$$\delta_- = \frac{4}{3} \left( 1 - \sqrt{1 - \frac{3}{2}\delta_c} \right) \quad (87)$$

is the smaller root of the quadratic equation

$$\delta - \frac{3}{8}\delta^2 - \delta_c = 0. \quad (88)$$

Then, using (83) with  $K = 4$  and (84), we obtain

$$\beta(M) = \frac{1}{\pi^2} \frac{\mu^3}{\sigma^7} \int_{\delta_-}^{4/3} d\delta \left( \delta - \frac{3}{8}\delta^2 - \delta_c \right)^\gamma \delta^3 \exp \left( -\frac{\delta^2}{2\sigma^2} \right). \quad (89)$$

The value of the critical collapse threshold  $\delta_c$  depends on the shape of the collapsing curvature power spectrum [63] (see also [57, 64]). In appendix A, we outline the calculation procedure. For a broad power spectrum that could be approximated by (65), one finds  $\delta_c \sim 0.56$  [63].

## Comparison

To compare these two methods, we can use the toy-model spectrum (65). In this model, the function  $\beta(M)$  may be approximated by a similar top-hat profile

$$\beta(M) = \beta_0 \Theta(M - M_{\min}) \Theta(M_{\max} - M), \quad (90)$$

where the height  $\beta_0$  can be estimated using either (82) or (89). By way of example, we will use  $\gamma = 0.36$ ,  $\delta_c = 0.56$ , and  $\sigma = (4/9)\sqrt{\mathcal{P}_0/2}$  with  $\mathcal{P}_0 = 0.2$  or  $0.4$ . Then, using (89) we obtain  $\beta_0 = 1.536 \cdot 10^{-7}$  for  $\mathcal{P}_0 = 0.2$  and  $3.429 \cdot 10^{-5}$  for  $\mathcal{P}_0 = 0.4$ . In contrast, using (82) we obtain  $\beta_0 = 3.441 \cdot 10^{-5}$  and  $2.489 \cdot 10^{-3}$  for  $\mathcal{P}_0 = 0.2$  and  $\mathcal{P}_0 = 0.4$ , respectively. Hence, the Press-Schechter prediction based on Eq. (82) is by a factor of 100 larger than the prediction of the CCP formalism based on Eq. (89). In the following, we will use the more conservative CCP formalism.

**Nota Bene:** The height  $\beta_0$  decreases very quickly with decreasing  $\mathcal{P}_0$ . For example, using (89) we find for  $\mathcal{P}_0 = 0.08$ . For the values of  $\mathcal{P}_0$  below 0.08, e.g., 0.04, the value of  $\beta_0$  becomes insignificant.

## 5.2 PBH abundance

The abundance of PBHs with mass in the interval  $(M, M + dM)$  related to the total dark matter (DM) today is defined as [56, 61, 65, 66, 67, 68]

$$\frac{d\Omega_{\text{PBH},0}}{\Omega_{\text{DM},0}} = f_{\text{PBH}} d \ln M. \quad (91)$$

Here,  $f_{\text{PBH}}$  is the mass-dependent PBH fraction defined as

$$f_{\text{PBH}} \equiv \frac{\rho_{\text{PBH},0}}{\Omega_{\text{DM},0} \rho_{\text{crit}}} = \frac{\rho_{\text{PBH},f}}{\Omega_{\text{DM},0} \rho_{\text{crit}}} \left( \frac{a_f}{a_0} \right)^3 = \frac{\beta(M) \rho_{\text{rad},f}}{\Omega_{\text{DM},0} \rho_{\text{crit}}} \left( \frac{a_f}{a_0} \right)^3, \quad (92)$$

where  $\Omega_{\text{DM},0}$  is the fraction of DM today. We have taken into account that PBHs behave like matter, i.e.,  $\rho_{\text{PBH},0} a_0^3 = \rho_{\text{PBH},f} a_f^3$  and that the PBH density at the formation time is a fraction  $\beta(M)$  of the total background density  $\rho_{\text{rad},f}$ . Substituting  $\rho_{\text{rad},f}$  from entropy conservation (72),  $a_f/a_0$  from (74), and  $q_f/q_0$  from (75), we obtain

$$f_{\text{PBH}} = \frac{\beta(M) \Omega_{\text{rad},0}^{3/4}}{\Omega_{\text{DM},0}} \left( \frac{g_{*,0}}{g_{*,f}} \right)^{1/4} \left( \frac{M_0}{M} \right)^{1/2}, \quad (93)$$

where

$$M_0 = 4\pi M_{\text{Pl}}^2 / H_0 \quad (94)$$

is the mass of the present cosmological horizon. If we use  $g_{*,0} = 3.36$ ,  $\Omega_{\text{rad},0} = 10^{-5}$ ,  $\Omega_{\text{DM},0} = 0.265$ ,  $H_0 = 70 \text{ km s}^{-1} \text{Mpc}^{-1}$ , and  $M_\odot = 2 \cdot 10^{30} \text{ kg}$ , we find

$$f_{\text{PBH}} = \frac{\beta(M)}{1.67 \cdot 10^{-8}} \left( \frac{M_\odot}{M} \right)^{1/2} \left( \frac{106.75}{g_{*,f}} \right)^{1/4}. \quad (95)$$

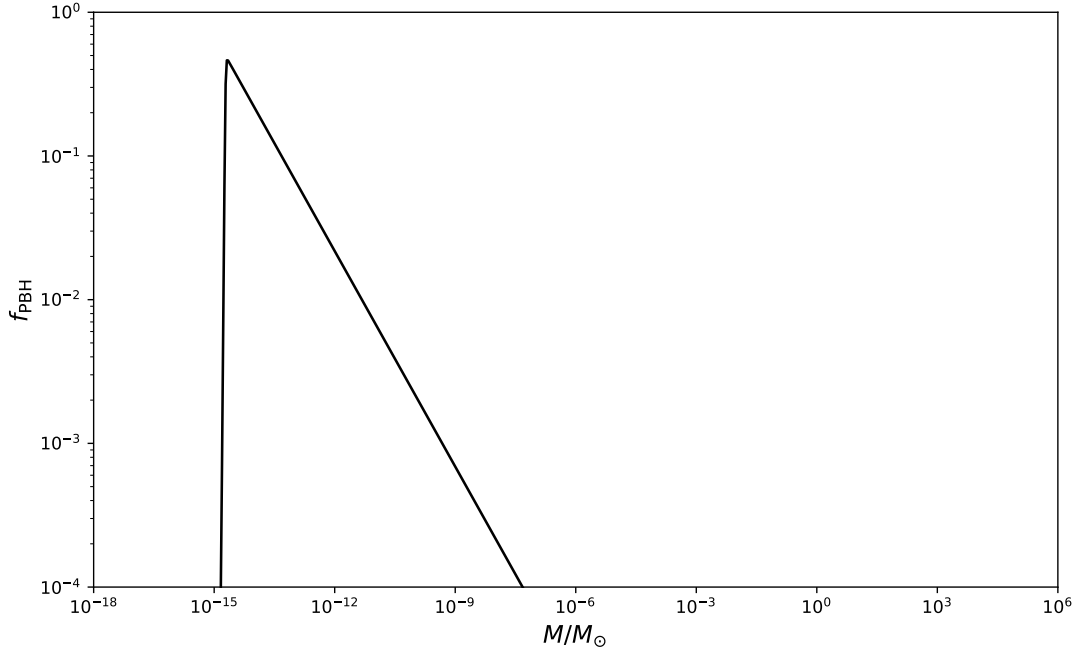


Figure 5: The fraction of PBH dark matter versus  $M$  for the flat power spectrum (65) with  $q_{\min} = 10^4 q_{\text{CMB}}$ ,  $q_{\max} = 10^{15} q_{\text{CMB}}$ , and  $\mathcal{P}_0 = 0.08866$ .

### PBH abundance in the top-hat model

For an estimate based on the top-hat toy model, we use  $\beta(M)$  defined by (90) with mass range  $(M_{\min}, M_{\max})$  defined by (78) and (79) and  $\beta_0$  calculated in Sec. 5.1 for a chosen  $\mathcal{P}_0$ . It is clear that the values  $\mathcal{P}_0$  and  $q_{\max}$  (or the corresponding  $M_{\min}$ ) are decisive since  $\beta(M)$  is extremely sensitive to  $\mathcal{P}_0$  and since  $f_{\text{PBH}}$  peaks just above  $M_{\min}$ .

As an example, we take  $q_{\max} = 10^{15} q_{\text{CMB}}$  corresponding to  $M_{\min} = 1.91 \cdot 10^{-15} M_{\odot}$  and we use the approximate expression (90) with  $\beta_0$  estimated using (89). Then, for  $\mathcal{P}_0 = 0.2$  we find  $\beta_0 = 1.536 \cdot 10^{-7}$  and  $f_{\text{PBH,peak}} = 2.105 \cdot 10^8$ , whereas for  $\mathcal{P}_0 = 0.08866$  we obtain  $\beta_0 = 3.6537 \cdot 10^{-16}$  and  $f_{\text{PBH,peak}} = 0.50061$ . In Fig. 5, we plot the fraction of PBH dark matter as a function of  $M$  at the formation time for the top-hat power spectrum (65) with height  $\mathcal{P}_0 = 0.08866$ . The choice of  $q_{\max}$  in the top-hat profile is crucial since the position  $M_{\min}$  of the DM fraction peak is proportional to  $1/q_{\max}^2$  (Eq. (78)). There exists a natural cutoff at about  $q_{\max} \sim 10^{17} q_{\text{CMB}}$  which corresponds to  $M_{\min} \simeq 10^{-18} M_{\odot} \simeq 10^{15}$  g. The PBHs of masses smaller than this would have evaporated completely until today.

### PBH abundance in the PLLS and Tachyon models

In Fig. 6, we plot the fraction of PBH dark matter as a function of  $M$  for the power spectra approximated by equation (57) for both the PLLS and the Tachyon models. The theoretical curves correspond to the power spectra calculated using specifically tuned input parameters listed in Table 2. The requirement that the PBH abundance is outside the regions constrained by observations dictates the choice of input parameters.

Table 2: Input parameters corresponding to  $f_{\text{PBH}}(M)$  plotted in Fig. 6

Model	$V_0[M_{\text{Pl}}^4]$	$\lambda \times 10^6$	$\phi_0[M_{\text{Pl}}]$	$\eta_{\text{in}}$	$\phi_{\text{in}}[M_{\text{Pl}}]$	$\delta_c$	Line Style
<b>PLLS</b> $\alpha = 1.5$	$10^{-16}$	7.5490	0.835370	$-1.4500 \times 10^{-8}$	5.2200	0.51	full
		7.5400	0.835370	$-2.8174 \times 10^{-7}$	5.2500		dashed
		7.5400	0.835370	$-2.8174 \times 10^{-7}$	5.3000		dash-dotted
		3.9523	0.895870	$-1.0089 \times 10^{-3}$	5.1124		long dashed
<b>Tachyon</b>	$10^{-16}$	7.5020	0.259500	$-6.1200 \times 10^4$	1.1000	0.56	full
					1.1005		dashed
					1.1010		dash-dotted
		7.6000	0.259831	$-5.3625 \times 10^4$	1.0520		long dashed

The critical collapse thresholds  $\delta_c$  are calculated for each model using the procedure described in appendix A. The variations of input parameters and initial values in the ranges given in Table 2 do not substantially affect the shape of the spectra, so the variations of the corresponding critical collapse thresholds are insignificant. The obtained values are  $\delta_c = 0.51$  for the PLLS model and  $\delta_c = 0.56$  for the Tachyon model spectra. The fraction of PBH is calculated using Eqs. (89) and (95), with  $\sigma$  and  $\mu$  obtained from (62) and (63), respectively. The data for the constraints are from Ref. [17].

The PLLS model with the set of parameters in Table 2 predicts the PBH fraction peaks in the observationally allowed windows of masses between  $10^{-13}$  and  $10^{-10}$  and between  $10^{-6}$  and  $10^{-4}$  solar masses. The Tachyon model, with the set of parameters in Table 2, predicts experimentally allowed PBH abundance today in a broad mass range from  $10^{-16}$  to  $10^6$  solar masses, except for the special case (long dashed black line on Fig. 6) with the allowed masses between  $10^{-14}$  and  $10^{-10}$  solar masses.

For a DM prediction, we need the integrated PBH dark matter fraction. To this end, we use the definition (91) so the integrated PBH dark matter abundance in the mass interval  $(M_{\text{min}}, M_{\text{max}})$  related to the total DM fraction is given by

$$F_{\text{PBH}} = \int_{M_{\text{min}}}^{M_{\text{max}}} f_{\text{PBH}} \frac{dM}{M}. \quad (96)$$

The results for both models are given in Table 3 for each set of parameters listed in Table 2. The PBH contribution to DM today could be significant and, in particular cases, even sufficient to account for the total DM. However, it is important to stress that the parameterization of the Tachyon model that leads to  $F_{\text{PBH}} = 0.978$  corresponds to the spectrum not supported by the CMB observational data in the vicinity of the CMB pivot scale  $q_{\text{CMB}}$ .

## 6 Summary and conclusions

We have analyzed the PBH production in the early universe in the top-hat toy model and two  $k$ -essence models of inflation. The analysis of the top-hat toy model reveals that the Press-Schechter prediction for the PBH mass fraction  $f_{\text{PBH}}$  based on Eq. (82) is by a factor of 100 larger than the prediction of the CCP formalism based on Eq. (89). For this reason, we have employed the more conservative CCP formalism in calculating  $f_{\text{PBH}}$  for realistic power spectra.

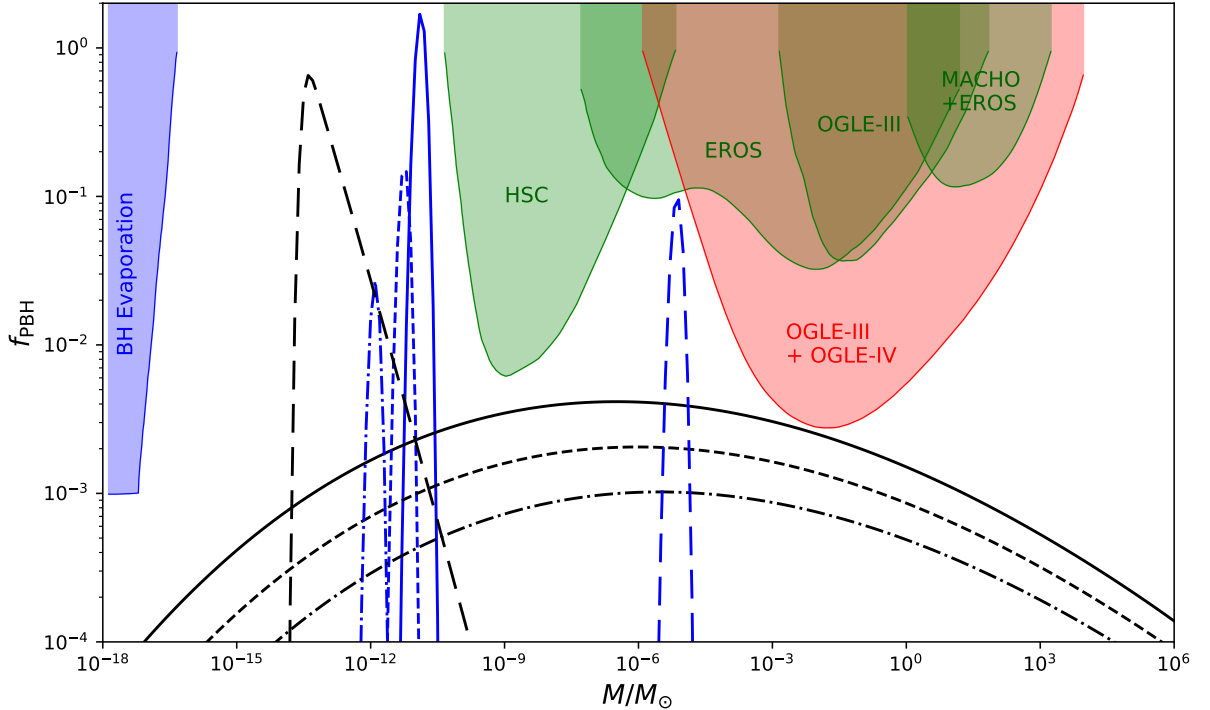


Figure 6: The fraction of PBH dark matter versus the PBH mass  $M$  in the PLLS model (blue lines) and the Tachyon model (black lines) together with observational constraints. The corresponding input parameters and initial values are listed in Table 2. The green contours mark the limits determined by EROS [12], OGLE-III [13], Hyper Suprime-Cam (HSC) [15], and MACHO+EROS [16]. The orange contour marks the constraints by OGLE-III + OGLE-IV [17].

Besides, the analysis of the top-hat model shows that the PBH abundance is very sensitive to the height of the power spectrum. The top-hat power spectrum with height equal to or above 0.2 yields too large PBH abundance with  $f_{\text{PBH}} \gg 1$  whereas a height below 0.08 yields a small peak value of  $f_{\text{PBH}}$  less than 0.02.

Regarding the PLLS and Tachyon models, we have demonstrated that it is possible to obtain a significant PBH DM fraction by fine-tuning the input parameters,  $V_0$ ,  $\phi_0$ ,  $\lambda$ , and initial conditions for the background equations. However, the normalization requirement for the spectrum to fit the observational value at the pivot CMB scale constrains the tuning of these parameters. This normalization requirement can be easily implemented by utilizing the rescaling invariance [48].

The PBH abundance is fairly sensitive to the value of the critical collapse threshold  $\delta_c$ . We have found that the shape of the spectra in both models does not significantly change with slight variations in input parameters. As a consequence, the critical collapse threshold  $\delta_c$  is also not very sensitive to these variations. Hence, the values of  $\delta_c$  calculated for the spectra presented in Figs. 3 and 4 for the PLLS and the Tachyon model, respectively, could have been applied for each set of parameters presented in Table 2.

Our results for the PLLS model show that a suitable choice of input parameters different from those in Ref. [20] could yield a significant PBH abundance. For a chosen set of parameters yielding

Table 3: Integrated PBH DM fractions corresponding to  $f_{\text{PBH}}(M)$  plotted in Fig. 6

Model	$F_{\text{PBH}} [\%]$	Line Style
<b>PLLS</b> $\alpha = 1.5$	100	full blue
	9.0	dashed blue
	1.4	dash-dotted blue
	6.2	long dashed blue
<b>Tachyon</b>	10.6	full black
	5.3	dashed black
	2.6	dash-dotted black
	97.8	long dashed black

the power spectrum of Fig. 3, the PBH fraction has a few sharp peaks around the PBH mass  $M = 10^{-11} M_{\odot}$ . In contrast, the Tachyon model power spectrum of Fig. 4 predicts experimentally allowed PBH abundance today in a broad mass range (Fig. 6). In the PLLS model, the integrated PBH abundance of the highest peak (full blue line) in Fig. 6 could account for total DM. In the Tachyon model, the highest integrated contribution of PBHs to DM estimate is about 11% (full black line), except for a particular parameterization (long dashed black line) where the integrated PBH contribution may reach up to 98%. However, the latter result should not be taken seriously since the spectrum corresponding to this parameterization is not supported by the observational data near the CMB pivot scale.

## A The critical collapse threshold

The critical collapse threshold  $\delta_c$  for PBH formation depends on the shape of the curvature perturbation spectrum. The shape parameter  $\alpha$  describes the main features of the profile in the length-scale interval  $0 < r < r_m$  where PBHs form. Here, we outline the procedure for calculating  $\delta_c$  following Musco *et al.* [63].

The first step is to compute the value of the comoving length scale  $\hat{r}_m$  of the perturbation related to  $r_m$  via the coordinate transformation  $r = \hat{r} \exp \zeta(\hat{r})$ . To this end, we use the smoothed power spectrum  $\mathcal{P}_S(q, \tau)$  defined as

$$\mathcal{P}_S(q, \tau) = \frac{2\pi^2}{q^3} \mathcal{P}_S(q) T^2(q\tau), \quad (97)$$

where the transfer function  $T(x)$  is defined as

$$T(x) = 3 \frac{\sin(x/\sqrt{3}) - (x/\sqrt{3}) \cos(x/\sqrt{3})}{(x/\sqrt{3})^3}. \quad (98)$$

The conformal time interval  $\tau$  is, according to (50), approximately  $\tau = -1/aH$ . Now we assume that the scale  $\hat{r}_m$  is a factor of 10 to 100 larger than the comoving horizon radius  $1/(aH)$ . Hence, in Eq. (98) we may substitute  $-\hat{r}_m/p$  for  $\tau$ , where  $p$  is a constant of order  $10 \leq p \leq 100$  and, according to [63], the scale  $\hat{r}_m$  is a positive root of the function

$$I(x) = \int_0^\infty \frac{dy}{y} \left[ (y^2 - 1) \frac{\sin y}{y} + \cos y \right] \mathcal{P}_S(y/x) T^2(y/p). \quad (99)$$

As the next step, we compute the shape parameter  $\alpha$ . First, we find the linear Gaussian shape parameter  $\alpha_G$  using

$$\alpha_G = -\frac{1}{4} \left[ 1 + \frac{\int y dy \cos y \mathcal{P}_S(y/\hat{r}_m) T^2(y/p)}{\int dy \sin y \mathcal{P}_S(y/\hat{r}_m) T^2(y/p)} \right]. \quad (100)$$

Then, we compute the shape parameter  $\alpha$  by solving the algebraic equation

$$F(\alpha)(1 + F(\alpha))\alpha = 2\alpha_G, \quad (101)$$

where

$$F(\alpha) = \left( 1 - \frac{2}{5} \frac{e^{-1/\alpha} \alpha^{1-5/(2\alpha)}}{f(\alpha)} \right)^{1/2}, \quad (102)$$

with

$$f(\alpha) = \Gamma(5/(2\alpha)) - \Gamma(5/(2\alpha), 1/\alpha) \equiv \int_0^{1/\alpha} dt e^{-t} t^{5/(2\alpha)-1}. \quad (103)$$

Finally, we compute the threshold  $\delta_c$  as a function of  $\alpha$ . Up to a few percent precision, the threshold can be expressed as an analytic function

$$\delta_c(\alpha) = \frac{4}{15} \frac{e^{-1/\alpha} \alpha^{1-5/(2\alpha)}}{f(\alpha)}. \quad (104)$$

## Acknowledgments

This work is supported by the ICTP-SEENET-MTP project NT-03 Cosmology-Classical and Quantum Challenges and the COST action CA1810 “Quantum gravity phenomenology in the multi-messenger approach”. N. Bilić is indebted to E. Saridakis for valuable comments. M. Stojanović acknowledges the support by the Ministry of Science, Technological Development and Innovation of the Republic of Serbia under contract 451-03-137/2025-03/200113. D.D. Dimitrijević, G.S. Djordjević, and M. Milošević acknowledge the support by the same Ministry under contract 451-03-137/2025-03/200124. G.S. Djordjević and D.D. Dimitrijević acknowledge the support by the CEEPUS Program RS-1514-03-2223 “Gravitation and Cosmology”. G.S. Djordjević acknowledges the hospitality of the CERN-TH. N. Bilić acknowledges the hospitality of the Department of Physics, University of Niš, where a part of his work has been completed.

## References

- [1] Y. B. N. Zel'dovich I. D. Novikov, Soviet Astron. AJ, **10**, 602 (1967).
- [2] S. Hawking, Mon. Not. Roy. Astron. Soc. **152**, 75 (1971).
- [3] B. J. Carr and S. W. Hawking, Mon. Not. Roy. Astron. Soc. **168**, 399 (1974).
- [4] B. J. Carr, Astrophys. J. **201**, 1 (1975).
- [5] G. F. Chapline, Nature **253**.5489, 251 (1975).
- [6] B. Carr and F. Kuhnel, Annual Review of Nuclear and Particle Science **70**, 355 (2020) [arXiv:2006.02838 [astro-ph.CO]].
- [7] A. M. Green and B. J. Kavanagh, *Primordial Black Holes as a dark matter candidate*, J. Phys. G **48** (2021) 043001 [arXiv:2007.10722].

- [8] I. Musco, Phys. Rev. D **100**, 123524 (2019) [arXiv:1809.02127 [gr-qc]].
- [9] C. Germani and I. Musco, Phys. Rev. Lett. **122**, 141302 (2019) [arXiv:1805.04087 [astro-ph.CO]].
- [10] A. Escrivà, C. Germani and R. K. Sheth, Phys. Rev. D **101**, 044022 (2020) [arXiv:1907.13311 [gr-qc]].
- [11] B. Carr, K. Kohri, Y. Sendouda and J. Yokoyama, Rept. Prog. Phys. **84**, 116902 (2021) [arXiv:2002.12778 [astro-ph.CO]].
- [12] P. Tisserand *et al.*, Astron. Astrophys. 469, 387–404 (2007).
- [13] L. Wyrzykowski *et al.*, Mon. Not. R. Astron. Soc. 416, 2949–2961 (2011).
- [14] K. M. Belotsky *et al.*, Mod. Phys. Lett. A **29**, 1440005 (2014) [arXiv:1410.0203 [astro-ph.CO]]; K. M. Belotsky *et al.*, Eur. Phys. J. C **79**, 246 (2019) [arXiv:1807.06590 [astro-ph.CO]].
- [15] H. Niikura *et al.*, Nature Astronomy 3, 524–534 (2019).
- [16] T. Blaineau *et al.*, Astron. Astrophys. 664, A106 (2022).
- [17] P. Mróz *et al.*, Nature **632**, no.8026, 749-751 (2024) [arXiv:2403.02386 [astro-ph.GA]].
- [18] C. Armendariz-Picon, V. F. Mukhanov and P. J. Steinhardt, Phys. Rev. Lett. **85** (2000) 4438 [arXiv:astro-ph/0004134].
- [19] C. Armendariz-Picon, T. Damour and V. F. Mukhanov, Phys. Lett. B **458** (1999) 209 [arXiv:hep-th/9904075].
- [20] T. Papanikolaou, A. Lymeris, S. Lola and E. N. Saridakis, JCAP **03** (2023), 003 [arXiv:2211.14900 [astro-ph.CO]].
- [21] C. F. S. Pereira, D. C. Rodrigues, J. C. Fabris and M. E. Rodrigues, Phys. Rev. D **109**, 044011 (2024) [arXiv:2309.10963 [gr-qc]]; C. F. S. Pereira *et al.*, Class. Quant. Grav. **42**, 015001 (2025) [arXiv:2405.07455 [gr-qc]]; C. F. S. Pereira *et al.*, Phys. Rev. D **111**, 084025 (2025) [arXiv:2409.09182 [gr-qc]]; C. F. S. Pereira *et al.*, Phys. Rev. D **111**, 124005 (2025) [arXiv:2503.09920 [gr-qc]].
- [22] M. Y. Khlopov, Res. Astron. Astrophys. **10**, 495-528 (2010) [arXiv:0801.0116 [astro-ph]]; M. Khlopov, Symmetry **16**, 1487 (2024).
- [23] J. Garcia-Bellido and E. Ruiz Morales, Phys. Dark Univ. **18**, 47-54 (2017) [arXiv:1702.03901 [astro-ph.CO]].
- [24] K. Kannike, L. Marzola, M. Raidal and H. Veermäe, JCAP **09**, 020 (2017) [arXiv:1705.06225 [astro-ph.CO]].
- [25] C. Germani and T. Prokopec, Phys. Dark Univ. **18**, 6-10 (2017) [arXiv:1706.04226 [astro-ph.CO]].
- [26] A. Y. Kamenshchik, A. Tronconi, T. Vardanyan and G. Venturi, Phys. Lett. B **791**, 201-205 (2019) [arXiv:1812.02547 [gr-qc]].
- [27] M. Fairbairn and M. H. G. Tytgat, Phys. Lett. B **546**, 1 (2002) [hep-th/0204070];
- [28] A. V. Frolov, L. Kofman and A. A. Starobinsky, Phys. Lett. B **545**, 8 (2002) [hep-th/0204187];
- [29] G. Shiu and I. Wasserman, Phys. Lett. B **541**, 6 (2002) [hep-th/0205003];

- [30] M. Sami, P. Chingangbam and T. Qureshi, Phys. Rev. D **66**, 043530 (2002) [hep-th/0205179];
- [31] G. Shiu, S. H. H. Tye and I. Wasserman, Phys. Rev. D **67**, 083517 (2003) [hep-th/0207119]; P. Chingangbam, S. Panda and A. Deshamukhya, JHEP **0502**, 052 (2005) [hep-th/0411210]; S. del Campo, R. Herrera and A. Toloza, Phys. Rev. D **79**, 083507 (2009) [arXiv:0904.1032]; S. Li and A. R. Liddle, JCAP **1403**, 044 (2014) [arXiv:1311.4664].
- [32] L. Kofman and A. D. Linde, JHEP **0207**, 004 (2002) [hep-th/0205121].
- [33] J. M. Cline, H. Firouzjahi and P. Martineau, JHEP **0211**, 041 (2002) [hep-th/0207156].
- [34] F. Salamate, I. Khay, A. Safsafi, H. Chakir and M. Bennai, Mosc. Univ. Phys. Bull. **73** 405 (2018).
- [35] N. Barbosa-Cendejas, R. Cartas-Fuentevilla, A. Herrera-Aguilar, R. R. Mora-Luna and R. da Rocha, JCAP. **2018** 005 (2018) [hep-th/1709.09016].
- [36] D. M. Dantas, R. da Rocha and C. A. S. Almeida, Phys. Lett. B. **782** 149 (2018) [hep-th/1802.05638].
- [37] D. A. Steer and F. Vernizzi, Phys. Rev. D **70**, 043527 (2004) [hep-th/0310139].
- [38] N. Bilic, D. D. Dimitrijevic, G. S. Djordjevic, M. Milosevic and M. Stojanovic, JCAP **08**, 034 (2019) [arXiv:1809.07216 [gr-qc]].
- [39] A. Y. Kamenshchik, A. Tronconi and G. Venturi, JCAP **01**, 051 (2022) [arXiv:2110.08112 [gr-qc]].
- [40] B. Li, C. Chen and B. Wang, Phys. Lett. B **848**, 138365 (2024) [arXiv:2307.03747 [astro-ph.CO]].
- [41] N. Bilić and G. B. Tupper, Central Eur. J. Phys. **12**, 147 (2014) [arXiv:1309.6588 [hep-th]].
- [42] N. Bilić, S. Domazet and G. Djordjevic, Class. Quant. Grav. **34**, 165006 (2017) [arXiv:1704.01072 [gr-qc]].
- [43] N. Bilic, D. Dimitrijevic, G. Djordjevic and M. Milosevic, Int. J. Mod. Phys. A **32**, 1750039 (2017) [arXiv:1607.04524 [gr-qc]].
- [44] M. Stojanovic, N. Bilic, D. D. Dimitrijevic, G. S. Djordjevic and M. Milosevic, Int. J. Mod. Phys. A **38**, 2343003 (2023) [arXiv:2306.02423 [gr-qc]].
- [45] G. W. Gibbons, Class. Quant. Grav. **20**, S321 (2003) [hep-th/0301117].
- [46] A. Sen, JHEP **9910**, 008 (1999) [hep-th/9909062].
- [47] S. E. Shandera and S.-H. H. Tye, JCAP **0605**, 007 (2006) [hep-th/0601099].
- [48] N. Bilić, D. D. Dimitrijević, G. S. Djordjevic, M. Milošević and M. Stojanović, Universe **11**, 128 (2025) [arXiv:2502.06456 [gr-qc]].
- [49] J. Garriga and V. F. Mukhanov, Phys. Lett. B **458**, 219-225 (1999) [arXiv:hep-th/9904176 [hep-th]].
- [50] N. R. Bertini, N. Bilic and D. C. Rodrigues, Phys. Rev. D **102**, 123505 (2020) [erratum: Phys. Rev. D **105**, 129901 (2022)] [arXiv:2007.02332 [gr-qc]].
- [51] A. De and R. Mahbub, Phys. Rev. D **102**, 123509 (2020) [arXiv:2010.12685 [astro-ph.CO]].
- [52] T. S. Bunch and P. C. W. Davies, Proc. Roy. Soc. Lond. A **360**, 117-134 (1978).
- [53] D. Wands, K. A. Malik, D. H. Lyth and A. R. Liddle, Phys. Rev. D **62**, 043527 (2000) [arXiv:astro-ph/0003278 [astro-ph]].

- [54] V. De Luca, G. Franciolini and A. Riotto, *Phys. Lett. B* **807**, 135550 (2020) [arXiv:2001.04371 [astro-ph.CO]].
- [55] E. W. Kolb and M. S. Turner, *The Early Universe*, Addison and Wesley, vol. 69. 1990, 10.1201/9780429492860.
- [56] M. Sasaki, T. Suyama, T. Tanaka and S. Yokoyama, *Class. Quant. Grav.* **35**, 063001 (2018) [arXiv:1801.05235 [astro-ph.CO]].
- [57] N. Bhaumik and R. K. Jain, *JCAP* **01**, 037 (2020) [arXiv:1907.04125 [astro-ph.CO]]
- [58] Yogesh and A. Mohammadi, *Astrophys. J.* **986**, 35 (2025) [arXiv:2501.01867 [gr-qc]].
- [59] <https://mathworld.wolfram.com/Erfc.html>
- [60] J. C. Niemeyer and K. Jedamzik, *Phys. Rev. Lett.* **80**, 5481-5484 (1998) [arXiv:astro-ph/9709072 [astro-ph]].
- [61] S. Young, I. Musco and C. T. Byrnes, *JCAP* **11**, 012 (2019) [arXiv:1904.00984 [astro-ph.CO]].
- [62] T. Koike, T. Hara and S. Adachi, *Phys. Rev. Lett.* **74**, 5170-5173 (1995) [arXiv:gr-qc/9503007 [gr-qc]].
- [63] I. Musco, V. De Luca, G. Franciolini and A. Riotto, *Phys. Rev. D* **103**, 063538 (2021) [arXiv:2011.03014 [astro-ph.CO]].
- [64] I. Dalianis, A. Kehagias and G. Tringas, *JCAP* **01**, 037 (2019) [arXiv:1805.09483 [astro-ph.CO]].
- [65] K. Inomata, M. Kawasaki, K. Mukaida, Y. Tada and T. T. Yanagida, *Phys. Rev. D* **96**, 043504 (2017) [arXiv:1701.02544 [astro-ph.CO]].
- [66] G. Ballesteros and M. Taoso, *Phys. Rev. D* **97**, 023501 (2018) [arXiv:1709.05565 [hep-ph]].
- [67] C. T. Byrnes, M. Hindmarsh, S. Young and M. R. S. Hawkins, *JCAP* **08**, 041 (2018) [arXiv:1801.06138 [astro-ph.CO]].
- [68] S. Pi, Y. l. Zhang, Q. G. Huang and M. Sasaki, *JCAP* **05**, 042 (2018), [arXiv:1712.09896 [astro-ph.CO]].